

## Complex particle emission from decaying regions of high excitation formed in $^{12}\text{C}$ induced reactions on $^{197}\text{Au}$ at $E/A = 30$ MeV

D. J. Fields, W. G. Lynch, C. B. Chitwood, C. K. Gelbke, M. B. Tsang, H. Utsunomiya, and J. Aichelin\*

*National Superconducting Cyclotron Laboratory, Michigan State University, East Lansing, Michigan 48824*

(Received 9 July 1984)

Energy spectra of complex nuclei ( $Z_f = 5-10$ ) emitted in  $^{12}\text{C} + ^{197}\text{Au}$  collisions at  $E/A = 30$  MeV were measured at angles significantly larger than the grazing angle. The angular dependence of these energy spectra gives clear evidence for the emission of these complex fragments prior to the attainment of statistical equilibrium of the compound nucleus. The qualitative features of the data are rather well described by assuming that complex fragments are emitted from a localized region of high excitation which is in the process of equilibration with the surrounding cold nuclear matter or, alternatively, that the target nucleus is shattered into several fragments by the incoming projectile.

### I. INTRODUCTION

The emission of complex nuclei ( $Z_f > 2$ ) in processes different from binary fission was first observed in high and intermediate energy hadron-nucleus collisions<sup>1-7</sup> and has been associated with the most violent of these reactions. More recently, similar processes have been observed in nucleus-nucleus collisions over a large range of incident energies.<sup>8-14</sup> A number of models have been proposed to explain these observations, including the direct cleavage of the target nucleus by the incident projectile,<sup>15,16</sup> sequential<sup>17</sup> and nonsequential<sup>18-21</sup> statistical emission from excited nuclear systems, the coalescence of nuclei from a hot gas of nucleons,<sup>22</sup> and the random shattering of a cold nucleus by the projectile.<sup>23</sup> The approximate power law dependence of the mass yields has been interpreted as a signature of statistical formation of clusters near the critical point in the liquid-gas phase diagram of nuclear matter.<sup>6,7</sup> This latter theory has spawned considerable theoretical interest.

Until now the existing data and their analysis could not distinguish between different models. For example, recent theoretical investigations indicate that a power law dependence of the mass yields is insufficient to establish the occurrence of critical phenomena, as the experimental dependence is equally well described by other very different models.<sup>17,22,23</sup> Systematic investigations of complex fragment emission over a wide range of incident energies and projectile-target combinations may provide an opportunity to study the underlying decay mechanisms in greater detail and to distinguish between conflicting interpretations. Specifically, the differential cross sections contain information that can considerably constrain reaction models which describe the emission of intermediate mass fragments.

In this paper we present energy spectra of intermediate mass nuclei measured for  $^{12}\text{C}$  induced reactions on  $^{197}\text{Au}$  at  $E/A = 30$  MeV. Energy integrated cross sections measured in this experiment have been published in a prior communication.<sup>14</sup> Section II provides a brief summary of the pertinent experimental details. In Sec. III, the data are presented and discussed in terms of a moving source

parametrization. In Sec. IV, the data are compared to model calculations which assume the statistical emission from a highly excited subsystem that is in the process of equilibration with the remainder of the composite system. In Sec. V, the experimental cross sections are compared with an alternative model which assumes that the incoming projectile shatters the cold target nucleus into several fragments.<sup>24</sup> A summary and conclusions are given in Sec. VI. Details concerning the model calculations are given in the appendices.

### II. EXPERIMENTAL DETAILS

The experiment was performed at the K500 cyclotron of the National Superconducting Cyclotron Laboratory of Michigan State University. A  $0.6 \text{ mg/cm}^2$   $^{197}\text{Au}$  target was bombarded with a 360 MeV  $^{12}\text{C}$  beam. Reaction products were detected with a three-element telescope subtending a solid angle of 5 msr and consisting of a 10 cm deep Frisch grid ion chamber<sup>25</sup> followed by two 0.4 mm silicon surface barrier detectors with  $450 \text{ mm}^2$  active areas. The ion chamber was operated at a pressure of about 80 Torr. Inclusive cross sections for the production of complex nuclei were measured at laboratory angles of  $30^\circ$ ,  $50^\circ$ ,  $70^\circ$ , and  $120^\circ$ . A two-dimensional  $\Delta E$ - $E$  histogram measured at a laboratory angle of  $70^\circ$  is shown in Fig. 1. Nuclei are clearly identified by element up to  $Z_f = 26$ . In the figure, the resolution is limited by the number of channels of the  $\Delta E$ - $E$  histogram. The actual data were taken at significantly higher channel resolution therefore allowing clear element identification between  $Z_f = 3-26$ . At more forward angles light elements were emitted with sufficient energies to punch through both silicon detectors causing serious spectral distortions for the lithium and beryllium energy spectra. The elemental yields could, nonetheless, be adequately determined for these cases.

The energy calibration of the silicon detectors was obtained by injecting a known amount of charge at the detector side of the preamplifier. The energy calibration of the ion chamber was obtained by using range-energy tables<sup>26</sup> to calculate the energy loss of the detected ions.

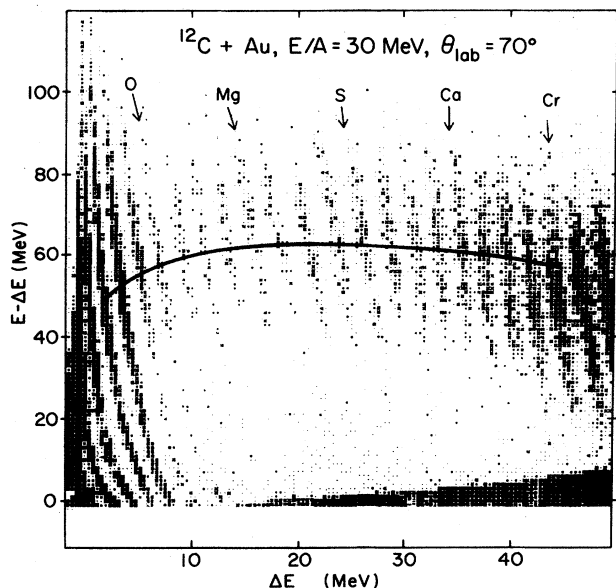


FIG. 1. A two-dimensional histogram of energy loss versus residual energy of intermediate mass fragments emitted at  $\theta_{\text{lab}}=70^\circ$  for  $^{12}\text{C}$  induced reactions on  $^{197}\text{Au}$ . For orientation, the solid line corresponds to the kinetic energy expected for very asymmetric fission.

The overall error of the energy calibration is believed to be smaller than 5%. Cross sections were determined from the known detector geometry, target thickness, and the integrated beam current. The uncertainty in the absolute cross sections is believed to be less than 20%.

### III. QUALITATIVE FEATURES OF THE DATA

Some of the qualitative features of the cross sections for the emission of complex nuclei at large angles have already been discussed in Ref. 14. Figure 2 shows the angle averaged cross sections for the emission of complex nuclei at angles significantly larger than the grazing angle for  $^{12}\text{C}$  induced reactions on  $^{197}\text{Au}$  at the incident energies of  $E/A=15$  and 30 MeV.<sup>14</sup> (In the computation of the average, the differential cross section  $d\sigma/d\theta$  was assumed to vary as  $ae^{b\theta}$ .) Over this energy range, the cross sections leading to the emission of fragments with element numbers between  $Z_f=3$  and 16 increase by more than one order of magnitude. The large cross sections observed for elements heavier than sulfur may correspond to the extreme tails of the element distributions resulting from fission either of the composite nucleus or the target residue. However, this has not yet been established experimentally. An alternative explanation has been proposed in Ref. 27 where it was pointed out that such an increase of cross sections with element mass may result if the system passes through a supersaturated vapor phase. More elaborate coincidence experiments may shed light on this interesting conjecture. It is, however, quite clear that the rapid rise of the cross sections for elements lighter than neon cannot be attributed to fission. In the remainder of this paper we focus our discussion on the production of these lighter elements.

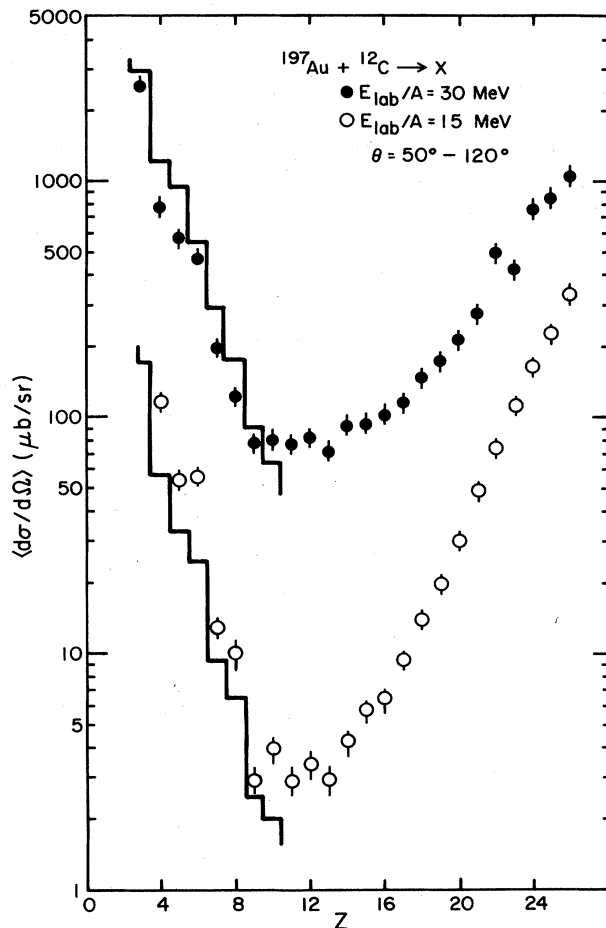


FIG. 2. Average element production cross sections measured for  $^{12}\text{C}$  induced reactions on  $^{197}\text{Au}$  at  $E/A=15$  and 30 MeV. The cross sections have been transformed to the compound nuclear center of momentum frame and are averaged over the angular interval of  $\theta_{\text{lab}}=50^\circ-120^\circ$ . The solid histogram shows the relative element yields calculated for the statistical emission from the compound nucleus (Ref. 14).

The energy integrated angular distributions for selected elements with  $4 \leq Z_f \leq 18$  produced in  $^{12}\text{C}$  induced reactions on  $^{197}\text{Au}$  at  $E/A=30$  MeV are shown in Fig. 3. For lighter elements, the angular distributions are forward peaked, indicating that these elements are emitted prior to the attainment of full statistical equilibrium of the composite nucleus. With increasing element number the angular distributions become less forward peaked, indicating higher degrees of equilibration of the emitting system. The angular distributions for elements heavier than magnesium are consistent with a constant  $d\sigma/d\theta$ , corresponding to the classical limit of emission from a long lived composite system at high angular momentum.

The corresponding energy spectra measured at laboratory angles of  $30^\circ$ ,  $50^\circ$ ,  $70^\circ$ , and  $120^\circ$  are shown in Fig. 4 for fragments with  $Z_f=5-10$ . At each scattering angle the energy spectra exhibit approximately exponential slopes which become steeper at more backward angles. The qualitative features of these energy spectra are similar to those observed over a large range of projectile energies for noncompound light particle emission in heavy ion induced

reactions.<sup>28-31</sup> These noncompound light particle energy spectra have been rather well described in terms of a Maxwellian distribution centered about a velocity intermediate between compound nucleus and projectile velocities. The success of such a parametrization for noncompound light particle emission indicates that the noncompound light particle velocities are randomized at most among a subset of the nucleons contained in the composite system.

Qualitative information concerning complex fragment emission may be obtained by fitting the energy spectra in terms of a simple moving source parametrization. For simplicity, we assume isotropic emission in the rest frame of the source with a spectral shape given by

$$\frac{d^2\sigma}{dE_{sx}d\Omega} = CE_{sx} \exp(-E_{sx}/T), \quad (1)$$

where  $E_{sx}$  is the kinetic energy in the rest frame of the source of the fragment when it is immediately outside of the source,  $C$  is a normalization constant, and  $T$ , the apparent "temperature," is a parameter representing the random velocity of the source nucleons. In this expression, we have chosen the preexponential factor proportional to the energy  $E_{sx}$ , which corresponds to the assumption of surface emission.<sup>32</sup> The nonrelativistic expression for the cross section in the laboratory rest frame is then given by

$$\frac{d^2\sigma}{dE_{lab}d\Omega} = C[(E_{lab} - V_x)E_{sx}]^{1/2} \exp(-E_{sx}/T),$$

where

$$E_{sx} = E_{lab} - V_x + E_0 - 2[E_0(E_{lab} - V_x)]^{1/2} \cos\theta_{lab}. \quad (2)$$

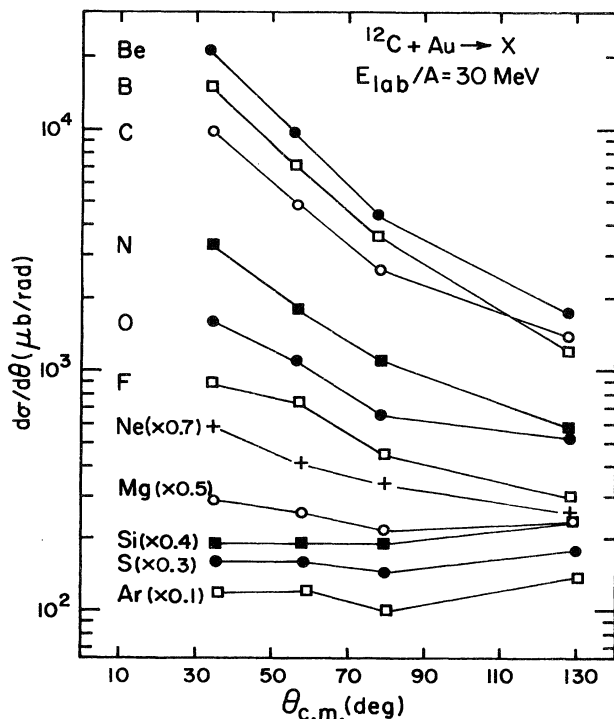


FIG. 3. Energy integrated center of mass cross sections for Be, B, C, N, O, F, Ne, Mg, Si, S, and Ar nuclei emitted in  $^{12}\text{C}$  induced reactions on  $^{197}\text{Au}$  at  $E/A = 30$  MeV.

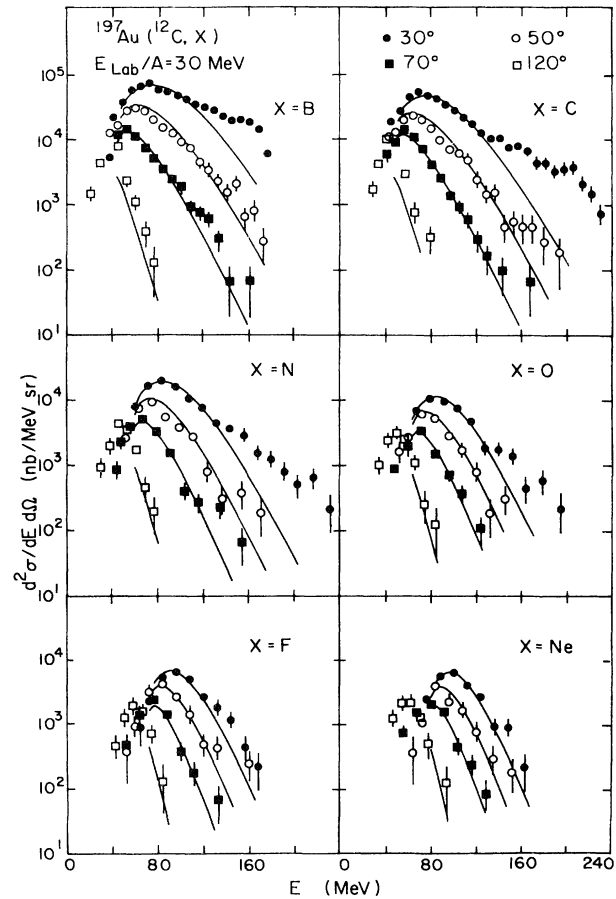


FIG. 4. Energy spectra of B, C, N, O, F, and Ne nuclei produced in  $^{12}\text{C}$  induced reactions on  $^{197}\text{Au}$  at  $E/A = 30$  MeV. The spectra were measured at the laboratory angles of  $30^\circ$ ,  $50^\circ$ ,  $70^\circ$ , and  $120^\circ$ . The solid lines correspond to fits with the moving source parametrization of Eq. (2).

Here,  $E_{lab}$  is the energy of the fragment in the laboratory frame,  $E_0 = m_f v_0^2/2$  is the kinetic energy of a fragment with mass  $m_f$  moving with the source velocity  $v_0$ , and  $V_x$  is a Coulomb correction which, for simplicity, is applied in the laboratory rest frame.<sup>28</sup> The characterization of the energy spectra in terms of this simple parametrization is shown by the solid lines in Fig. 4. It was not possible to obtain a satisfactory description of all energy spectra with a single choice of source parameters  $T$  and  $v_0$ . Therefore the solid lines in Fig. 4 correspond to independent fits for each element.

Some insight may be gained from the dependence of the best fit source parameters on the charge number  $Z_f$  of the emitted fragment. An estimate of the source size  $A_s$  may be obtained from  $v_0$  via the relationship  $A_s m_p = p/v_0$  by assuming that the source carries the entire projectile momentum  $p$  ( $m_p$  is the nucleon mass). The dependence of the estimated source size upon the charge number of the emitted fragment is shown in the upper part of Fig. 5. The apparent source temperatures are shown by the solid points in the lower part of the figure. For comparison, the temperature of an ideal Fermi gas at normal nuclear matter density formed by the fusion of the projectile on a

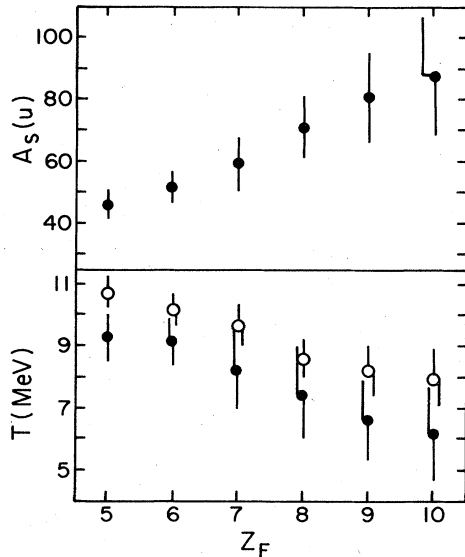


FIG. 5. Estimated source size and effective temperature parameters extracted from moving source fits to the energy spectra. The open points correspond to the upper limit of the temperature parameter consistent with energy and momentum conservation for a source of  $A_s$  nucleons, assuming an ideal Fermi gas at normal nuclear density.

target of  $(A_s - A_{\text{proj}})$  nucleons is indicated by the open points where  $A_s$  is given in the upper half of the figure. The general trend of the best fit parameters suggests that heavier particles originate from "colder" and slower and, hence, larger sources.

#### IV. STATISTICAL CALCULATION

The analysis of the previous section suggests that a subset of the available nucleons in a collision may act as the source of intermediate mass fragments and that the apparent size of this subset varies among the different fragments. This may be consistent with emission from a localized region of excitation which is evolving towards an equilibrium configuration provided: (1) the time scales for equilibration and particle emission are comparable, and (2) the hotter and smaller sources of the initial stages of the reaction emit relatively more of the lighter fragments than do the later fully equilibrated stages. Light particle coincidence data support the concept of particle emission from such a "hot spot."<sup>33</sup> Statistical calculations, discussed in this section and in more detail in Appendix A, suggest indeed that the hotter and smaller sources do favor the emission of the lighter fragments. This effect is illustrated in Fig. 6 where the dependence of the complex fragment emission rate upon the fragment charge for an emitting subsystem of 24 nucleons is compared to the corresponding rate from the compound nucleus.

In this calculation we assume that the entire projectile merges with some number of target nucleons to form a source of  $A_s$  nucleons. The total momentum and excitation energy of this source are calculated from energy and momentum conservation. (The entire projectile momentum is assumed either to remain with the source or to be

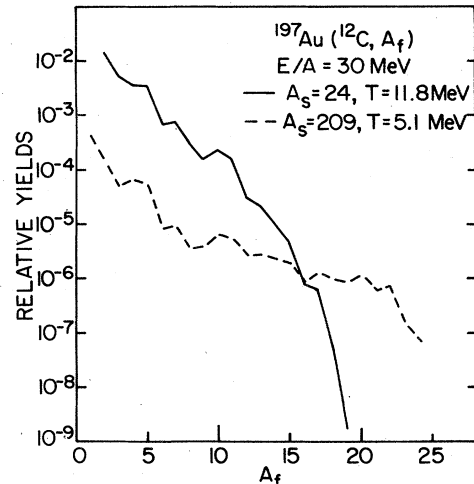


FIG. 6. The elemental yields for emission from a small very hot subsystem with  $A_s = 24$  and  $T = 11.8$  MeV (solid curve) are compared to the elemental yields for emission from the compound nucleus with  $A_s = 209$  and  $T = 5.1$  MeV (dashed curve). The temperatures have been calculated assuming an ideal Fermi gas at normal nuclear matter density.

carried away by the statistically emitted fragments.) Nucleons are accreted by the source from the target spectator. This process lowers the source velocity while converting translational energy associated with the center of mass motion of the source into excitation energy. During its entire evolution this idealized source emits particles at rates determined by the available phase space as calculated by an expansion of the Fermi gas level density assuming normal nuclear matter densities. These particle emission rates are calculated with a modified version of the statistical formalism of Friedman and Lynch.<sup>17,34</sup>

In the rest frame of the source, the distribution of kinetic energies of the emitted particles is taken to be given by Eq. (1). For the emission of heavier fragments the apparent temperatures of the energy spectra are considerably affected by the recoil of the emitting source and by the random Fermi momentum of the target participant nucleons which have been accreted to create the source. As a consequence, the apparent temperature parameters which describe the slopes of the energy spectra are not equal to the temperatures of the emitting source. The distribution given in Eq. (1), modified by these considerations, is then transformed to the laboratory with the Coulomb acceleration taking place in the center of momentum frame for the source plus target spectator. Simplifying approximations which are introduced in the kinematic transformations result in some sharp cutoffs in the distributions in the neighborhood of the Coulomb barrier. These cutoffs are removed by smearing the Coulomb barrier contained in the kinematic transformation over a range of values about the centroid. The final spectra are produced by summing the appropriately normalized spectral contributions which describe the fragment emission at each stage of the reaction.

The calculations are shown as solid lines in Fig. 7. In these calculations, the mean Coulomb barrier is taken to

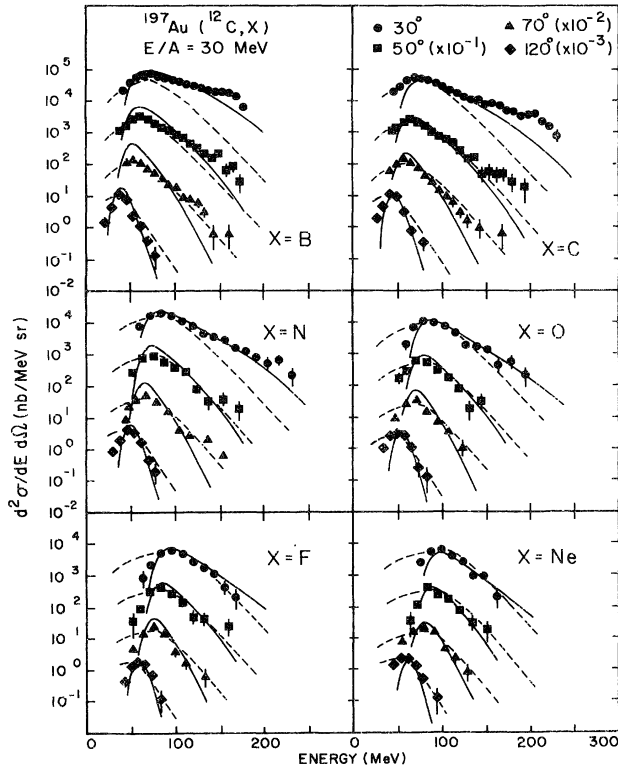


FIG. 7. Energy spectra of B, C, N, O, F, and Ne nuclei produced in  $^{12}\text{C}$  induced reactions on  $^{197}\text{Au}$  at  $E/A = 30$  MeV. The spectra were measured at the laboratory angles of  $30^\circ$ ,  $50^\circ$ ,  $70^\circ$ , and  $120^\circ$ . The solid lines correspond to calculations for the statistical decay of a region of high excitation as described in Appendix A. For these calculations, the recoil energy of the emitting source and the Fermi smearing of the source velocity have been taken into account. The dashed lines show the energy spectra calculated for the breakup of the cold target spectator matter as described in Appendix B.

be 0.9 of the touching sphere value. The Fermi energy is 38 MeV. The rate at which nucleons are accreted to the source from the cold target spectator region is taken to be a constant 2.0 nucleons per fm/c. It is important to note here that curves for all six elements were produced with the same set of input values, including the overall normalization, given by a reaction cross section of 350 mb.

In Fig. 8, the calculations are compared with the angular distributions of the energy integrated cross sections for different elements. Because of the rather crude treatment in the calculation of the exit channel Coulomb barriers, the experimental energy spectra were integrated only over the energy range for which the corresponding calculated cross section differed from zero. The calculation also predicts a factor of 3 increase in  $4 \leq Z_f \leq 7$  complex fragment cross sections as the bombarding energy is increased from  $E/A = 15$  to 30 MeV. This is less than the factor of 10 increase observed experimentally.

In general, the model calculation reproduces well the qualitative features of the experimental data at 30 MeV/nucleon. Many aspects of the reaction, e.g., a de-

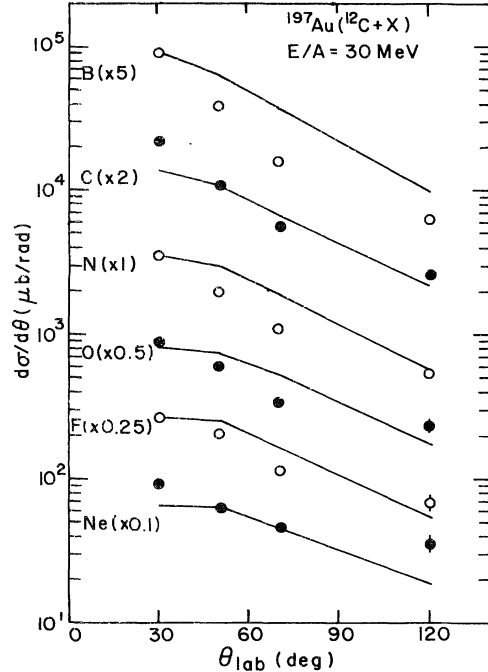


FIG. 8. Comparison of the energy integrated energy spectra with calculations which include recoil effects and Fermi smearing of the source velocities for the statistical decay of a region of high excitation. Because of the approximate treatment of the Coulomb barriers, the experimental energy spectra were only integrated over energies larger than the calculated thresholds.

tailed description of the hot spot formation process, shadowing, impact parameter averaging, thermal conductivity, and the influence of angular momentum, were neglected or treated very schematically by the present calculation. Additional calculations will be necessary to investigate the significance of these omissions.

## V. BREAKUP OF COLD TARGET SPECTATOR MATTER

For high energy nucleus-nucleus collisions, the emission of intermediate mass fragments is also well described by assuming the shattering of the cold spectator matter by the incident projectile.<sup>23,24</sup> We analyze the data by applying this alternative model in order to investigate whether ambiguities similar to those observed in high energy reactions exist as well at intermediate energies.

In this model the emission of complex fragments is viewed as a two-step, nonequilibrium process. In the first step the projectile collides with the target nucleus to form a hot spot in the region of geometrical overlap between target and projectile. The remaining nuclear matter (called the spectator matter) is assumed to remain cold. The hot spot is described in terms of its temperature and its total linear momentum parallel to the beam axis. In the second step of the reaction the hot spot is assumed to decay. Nucleons emerging from the hot spot penetrate into the spectator matter where they deposit energy and

linear momentum. As a consequence, local bonds are broken and a global destabilization of the spectator matter is assumed to take place. A fraction of the participant nucleons will escape while others will be captured by chunks of the spectator matter, thereby facilitating the dissocia-

tion of the destabilized spectator matter into nuclear fragments.

In the laboratory rest frame, the differential cross section for the emission of fragments of charge  $Z_f$  is parametrized in the following form:

$$\frac{d^3\sigma}{dE_{\text{lab}}d\Omega dZ_f} = C_0(Z_f) \int g(V_C) \delta^3(p_s - p_N - p_F) F_1(p_F) F_2(p_N) M_f p_L y d^3p_N d^3p_F dV_C, \quad (3)$$

where

$$\begin{aligned} \vec{p}_s &= (\vec{p}_L - M_f \vec{v}_{\text{c.m.}}) \\ &\times [1 - 2M_f V_C (\vec{p}_L - M_f \vec{v}_{\text{c.m.}})^2]^{1/2} \end{aligned}$$

and

$$y = [1 - 2M_f V_C / (\vec{p}_L - M_f \vec{v}_{\text{c.m.}})^2]^{1/2}.$$

The velocity of the spectator matter in the laboratory rest frame is denoted by  $v_{\text{c.m.}}$  and  $M_f$ ,  $p_L$ ,  $E_{\text{lab}}$ , and  $V_C$  are the mass, laboratory momentum, energy, and Coulomb barrier of the fragment. The distribution of the Fermi momentum in the spectator matter is preserved in this fast destabilization, and is reflected in the momentum distribution  $F_1(p_F)$  of the fragment, characterized by a width  $\Delta_f$  related in a straightforward manner to the Fermi momentum  $k_f$ . The momentum transferred by the hot spot nucleons,  $p_N$ , is described by the distribution  $F_2(p_N)$ , which is characterized by an average momentum  $\langle p \rangle$  and a temperature  $T$ . Since the fragments may be emitted from different sites in the target spectator matter an integration is performed over a distribution  $g(V_C)$  of Coulomb barriers. The maximum Coulomb barrier,  $V_{C,\text{max}}$ , is associated with the distance,  $R_{\text{max}}$ , between the centers of mass of a fragment and the spectator matter. This distance can be expressed by

$$R_{\text{max}} = \epsilon(R_t - R_f),$$

where  $R_t$  and  $R_f$  are the radii of the target and the fragment. Surface emission of a spherical fragment corresponds to a barrier  $V_{C,\text{max}}$  given by  $\epsilon=1$ . The relevant equations of the model are given in Appendix B; for a more detailed discussion we refer to Ref. 24.

For projectile energies of only a few tens of MeV per nucleon one should expect that the projectile is stopped within the target nucleus. As a consequence, the participant nuclear matter is expected to be more localized than at relativistic energies where the participant region is generally assumed to correspond to the entire region of overlap between target and projectile defined by straight line trajectories. This localization of the participant region results in a strong correlation between the velocity vectors of the participant nucleons and the velocity vectors of the emitted fragments, as is discussed in more detail in Appendix B. This correlation is incorporated in the calculations that are presented in the following.

The dashed lines in Fig. 7 compare the model calculations with the measured energy spectra. These calculations were performed by using the parameters  $T=5$  MeV,  $\langle p_N \rangle = 0.124$  MeV/ $c$ ,  $k_f = 240$  MeV/ $c$ ,  $v_{\text{c.m.}} = 0.019c$ , and  $\epsilon = 1.18$ . This results in maximum Coulomb barriers

of  $V_{C,\text{max}} = 50, 57, 63, 64, 71,$  and  $76$  MeV for B, C, N, O, F, and Ne fragments, respectively. These values correspond to the values expected for surface emission from slightly deformed fragments and are consistent with values used for the interpretation of complex fragment emission in high energy nucleus-nucleus collisions. For each element, the normalization constant  $C_0(Z_f)$  was adjusted independently. At high energies, these fragmentation cross sections have been interpreted in terms of the constraints imposed by charge conservation on a finite system of particles where the conserved charge is approximately that of the cold spectator matter.<sup>23,24</sup> When a similar procedure is attempted on the present data, a conserved charge of  $Z_0 = 20$  is obtained, which is much smaller than the charge of the target spectator (see also Appendix B). Within this model, this small value of the conserved charge might indicate that only a part of the spectator matter disintegrates to form fragments.

The model gives a satisfactory description of the overall trends of the energy spectra. For heavier elements, the calculated energy spectra extend to lower energies than observed experimentally, indicating that our simplified treatment of the Coulomb barriers is inadequate. Heavy fragments appear to be preferentially emitted from the surface region of the target residue. The model calculations do not reproduce the high energy tails of the energy spectra measured for B, C, and N at  $\theta_{\text{lab}} = 30^\circ$ . Further investigations will have to clarify whether these energy spectra contain contributions from more peripheral impact parameters and, consequently, different reaction mechanisms.

## VI. SUMMARY AND CONCLUSIONS

The energy spectra and angular distributions of intermediate mass fragments emitted in  $^{12}\text{C}$  induced reactions on  $^{197}\text{Au}$  at  $E/A = 30$  MeV exhibit clear evidence for the emission prior to the attainment of statistical equilibrium of the entire composite nucleus. For a given fragment, the angular dependence of the energy spectra were reasonably well described with a simple moving source parametrization. However, different source parameters were required to fit the data for different outgoing fragments. Assuming a thermal interpretation of the source parameters, the qualitative trends suggest that heavier fragments are emitted from larger and colder sources.

A rather satisfactory description of the differential cross sections was obtained by assuming that complex fragments are emitted from a localized region of high excitation which is in the process of equilibration with the surrounding cold target nuclear matter. The calculation

predicts that the hotter and smaller sources characteristic of the early stages of this reaction favor the emission of the lighter fragments relative to the emission from the fully equilibrated system. Because of the finite size of the emitting source, the kinetic energy of the recoiling source and the Fermi smearing of the source velocity should not be neglected. As a consequence, a purely thermal interpretation of the energy spectra is inadequate.

The energy spectra were also well described in terms of a model in which it is assumed that intermediate mass fragments originate from the cold target spectator matter which is shattered by the incident projectile. In this model the slopes of the energy spectra are not interpreted in terms of a temperature but, rather, in terms of the random velocity of the fragment caused by the Fermi motion of its constituents.

The success of the two models is most likely due to the fact that they both interpret the qualitative shapes of the energy spectra in terms of two different velocity components. One component is random in character. The other velocity component is primarily oriented along the direction of the beam axis. The relative importance of this oriented velocity component decreases with increasing fragment mass. In one model this effect is caused by the preferential emission of the heavier fragments from the cooler and larger sources characteristic of the later stages of the reaction. In the other model this effect is caused by the fact that the absorption of participant nucleons by heavier prefragments leads to smaller recoil velocities. On the basis of the present data, these two models cannot be distinguished.

The differential cross sections do indeed contain information which cannot be extracted from integrated cross sections. Quasistatic theories, such as those concerning phase transitions, have successfully reproduced the mass yields, but they must be reconciled with the preequilibrium aspects of the experimental cross sections. It is our belief that systematic measurements, including coincidence studies, with a variety of projectiles, targets, and energies will permit a discrimination among proposed reaction mechanisms for the production of intermediate mass fragments.

#### ACKNOWLEDGMENTS

The authors gratefully acknowledge discussions with W. A. Friedman. This work was supported in part by the National Science Foundation under Grant No. PHY 83-12245.

#### APPENDIX A: STATISTICAL EMISSION FROM AN EXCITED SUBSYSTEM

In this appendix, we generalize some expressions which have been used to describe particle emission from a highly excited compound nucleus to obtain approximations applicable to a system in which only a subset is at an elevated temperature. We start with the Weisskopf formula describing the emission of a particle  $x$  from a spherical source in the rest frame of that source

$$\frac{d^2N}{dE_{sx}dt} = f \frac{2S_x + 1}{\pi^2 h^3} M_x E_{sx} \sigma'_{inv} \exp(-\Delta S), \quad (A1)$$

where

$$E_{sx} = E_x - V_x.$$

Here,  $M_x$ ,  $S_x$ ,  $E_x$ , and  $V_x$  denote the mass, spin, kinetic energy released by the decay, and the Coulomb barrier for particle  $x$ . If particles are emitted by only a fraction  $f$  of the source surface area  $4\pi R_s^2$ , then the influence of shadowing is approximated by the multiplicative factor  $f$ . In the interest of clarity, we have introduced in Eq. (A1) the kinetic energy release,  $E_{sx}$ , corresponding to the placement of particle  $x$  immediately outside of the nucleus since that portion of the kinetic energy due to Coulomb repulsion is not part of the thermal energy governing the emission rate. This change of variables permits the thermal energy which is supplied by the source to be approximately decoupled from the Coulomb repulsion which is a property of the compound system. The inverse cross section is approximated by

$$\sigma'_{inv} = \pi R_{sx}^2 \theta(E_{sx}), \quad (A2)$$

where  $R_{sx} = r_0[(A_s - A_x)^{1/3} + A_x^{1/3}]$  and the theta function restricts  $E_{sx}$  to positive values. Here,  $A_s$  and  $A_x$  denote the number of nucleons of the emitting source (which may be smaller than the compound nucleus) and the emitted particle, respectively, and  $r_0 = 1.2$  fm. The Coulomb barrier  $V_x$  is taken to be that of the compound nucleus and is approximated as

$$V_x = \frac{\lambda e^2 Z_x (Z_{CN} - Z_x)}{r_C [A_x^{1/3} + (A_{CN} - A_s)^{1/3}]}, \quad (A3)$$

where  $r_C = 1.44$  fm;  $A_x$ ,  $Z_x$ , and  $A_{CN}$ ,  $Z_{CN}$  denote the mass and charge of the emitted particle and the compound nucleus. The factor  $\lambda < 1$  is an adjustable parameter to correct for deformation effects ( $\lambda$  is 0.9 for the calculations presented in this paper). The change in the entropy of the emitting source is given to second order by

$$\Delta S = \frac{-E_{sx} - B_{rx}}{T} + \frac{Z_x(\epsilon_p^* - T_p^\sigma) + N_x(\epsilon_n^* - T_n^\sigma)}{T} - \frac{(Z_x \epsilon_p^* + N_x \epsilon_n^* - E_{sx} - B_{rx})}{2T^2 [C_{vp}(Z_s - Z_x) + C_{vn}(N_s - N_x)]}, \quad (A4)$$

where  $B_{rx} = V_x + B_x$  and  $B_x$  denotes the separation energy of particle  $x$ ,  $T$  is the source temperature,  $C_{vp}$  and  $C_{vn}$  denote the specific heat for protons and neutrons, and  $N_s = A_s - Z_s$ ,  $N_x = A_x - Z_x$ . The excitation energy per nucleon and the entropy per nucleon of the proton and neutron components are denoted by  $\epsilon_p^*$ ,  $\sigma_p$  and  $\epsilon_n^*$ ,  $\sigma_n$ , respectively.

This excited subsystem is assumed to be formed by the fusion of the projectile nucleons with an equal number of target nucleons. This source accretes nucleons from the target spectator with an accretion rate,  $(dA_s/dt)_a$ , which may be time dependent; the velocity and excitation energy of the source is determined by energy and momentum conservation. Once the accretion rate is defined, the evolution of the source is given by  $(dA_s/dt)_a$  and by taking an ensemble average over the possible decay channels, which include the emission of excited nuclei according to the criteria established in Ref. 34. The total mass of the

source can be calculated from the rate equation

$$\frac{dA_s}{dt} = \left[ \frac{dA_s}{dt} \right]_a - \sum_x \frac{dN_x}{dt} A_x, \quad (\text{A5})$$

where the second term is due to particle emission, and the emission rate  $dN_x/dt$  is given by

$$\frac{dN_x}{dt} = \int_0^\infty \frac{d^2N_x}{dE_{sx}dt} dE_{sx}. \quad (\text{A6})$$

The equation for the rate of change of the source momentum is

$$\frac{dP_s}{dt} = -[P_s(t)/A_x(t)] \sum_x A_x \frac{dN_x}{dt}. \quad (\text{A7})$$

The rate of change of the excitation energy of the source is given by

$$\frac{dE^*}{dt} = - \sum_x \left[ \frac{dN_x}{dt} B_{rx} + \frac{d(E_k)_x}{dt} \right] + \frac{P_s^2}{2m_p A_s^2} \frac{dA_s}{dt} \quad (\text{A8})$$

and the average rate of kinetic energy loss by particle emission is given by

$$\frac{d(E_k)_x}{dt} = \int_0^\infty \frac{d^2N_x}{dE_{sx}dt} E_{sx} dE_{sx}. \quad (\text{A9})$$

The last term of Eq. (A8) takes into account the thermalization of center-of-mass motion of the source as it slows down. Once the source has expanded to include completely the spectator region, the accretion phase of the calculation ceases and the compound nuclear geometry is assumed for the subsequent decay. For Eqs. (A5)–(A9) the appropriate equations in this limit are achieved by setting the accretion rate to zero.

Equations (A1)–(A9) define the time evolution of the emitting source. There are, however, complications involving the treatment of the Coulomb barrier of the emitted particles and the acceleration of the emitted particles in the Coulomb field of the target residue. Since the Coulomb interaction is expected to affect primarily the low energy part of the energy spectra, we assume for simplicity that the final Coulomb acceleration takes place in a rest frame which moves with a velocity  $v_C$ , with respect to the laboratory, which is parametrized as

$$v_C = \frac{v_s A_s}{A_{\text{tot}}}, \quad (\text{A10})$$

where  $v_s$  is the velocity of the emitting system and  $A_{\text{tot}}$  is the number of nucleons in the composite system at the time of emission. The energy spectra in the laboratory rest frame are then generated as follows. The energy spectrum of Eq. (A1) is first transformed into the rest frame moving with the velocity  $v_C$  parallel to the beam axis. In this rest frame, the Coulomb repulsion is approximated by shifting the energy spectrum by the amount  $V_x$ .  $V_x$  was taken to be Gaussian distributed with a variance of  $(6 \text{ MeV})^2$  about an average provided by Eq. (A3) in order to smear out the influence of the sharp cutoff approximation used on the reaction cross section of Eq. (A2). As a

final step in the calculation, the resulting energy spectrum is transformed into the laboratory rest frame to obtain  $d^2N/(dE_{\text{lab}}dt)$ .

The recoil energy of the source can be included into the calculations by substituting  $E_{sx} = E_{fx} A_s / (A_s - A_x)$  into Eq. (A1), where  $E_{fx}$  is the energy of fragment  $x$  in the rest frame of the emitting source. The inclusion of the Fermi smearing of the source velocity may be done by calculating the mean square momentum of the target nucleons accreted by the source.<sup>35</sup> In first order, the resulting energy spectrum at energies large with respect to the Coulomb barrier is obtained by multiplying the particle spectrum in the rest frame of the source by the factor

$$C_x \exp[E_{fx} A_s / T(A_s - A_x) - E_{fx} / T_{\text{eff}}], \quad (\text{A11})$$

where  $T_{\text{eff}}$  is given by

$$T_{\text{eff}} = \frac{T}{A_s} (A_s - A_x) + \frac{k_F^2}{5m_p} A_x \frac{A_{st}(A_t - A_{st})}{(A_t - 1)A_s^2}. \quad (\text{A12})$$

Here,  $A_t$  and  $A_{st}$  denote the total number of target nucleons and the number of target nucleons accreted by the emitting source, respectively. The normalization constant,  $C_x$ , is determined by the condition that the emission rate of particle  $x$  remains unchanged. The influence of recoil energy and Fermi smearing corrections for  $^{10}\text{B}$  emitted to  $30^\circ$  and  $120^\circ$  from an equilibrating source is illustrated in the calculations of Fig. 9 for which a constant accretion rate of 2 nucleons/(fm/c) is assumed. The dashed line indicates calculations which include neither the Fermi smearing nor the source recoil correction. The dashed-dotted line shows the decrease in slope which occurs when source recoil corrections but not Fermi smearing are considered. With the addition of both Fermi smearing and source recoil corrections, the solid curve is obtained. It can be seen that the recoil energy and Fermi smearing corrections are nearly comparable in magnitude

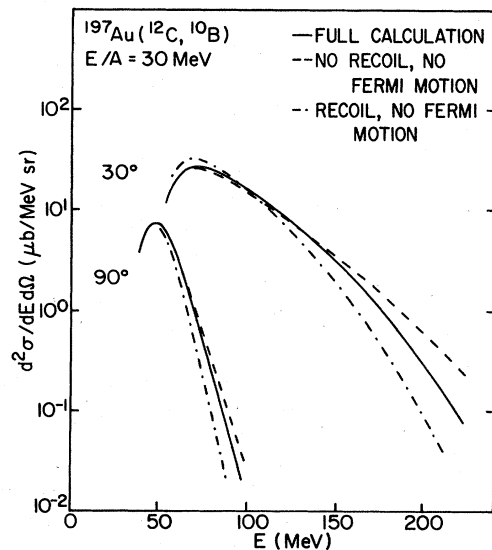


FIG. 9. Calculations showing the influence of Fermi smearing and source recoil corrections on the energy spectra  $^{10}\text{B}$  fragments emitted in  $^{12}\text{C}$  induced reactions on  $^{197}\text{Au}$  at  $E/A = 30$  MeV. See the text for a discussion of the curves.

and opposite in sign.

The final spectra were created by integrating  $d^2N/(dE_{\text{lab}}dt)$  over time and multiplying by the reaction cross section for the creation of the highly excited subsystem,  $\sigma_r$ . As shown in Fig. 10, the relative contributions to the spectra from the various stages of the reaction depend quite strongly upon the scattering angle. The dashed line indicates the spectra of  $^{12}\text{C}$  fragments emitted in the early stages of the reaction when the source is still quite small ( $A_x < 36$  nucleons). Emission from the early stages is kinematically focused to forward angles and contributes strongly to the yield of energetic fragments at forward angles. The spectra at more backward angles are quite strongly affected by emission from the later fully equilibrated stages indicated by the dotted-dashed line. The contributions from the different stages of the reaction blend together to form the final spectra indicated by the solid lines.

For the calculations presented in Figs. 7–10, a time independent accretion rate of 2 nucleons/(fm/c) was assumed and the influence of shadowing was neglected ( $f=1$ ). To indicate that the qualitative features of these calculations may be preserved in calculations incorporating alternative geometrical assumptions for the expansion, we discuss here a simple geometric description which includes shadowing and thermal expansion rate considerations. For simplicity the thermal source is assumed to expand with a constant velocity of expansion,  $v_t$ , radially (with radius  $R_t$ ) from a point on the surface of the composite system, which is assumed to be spherical with a radius  $R_{\text{tot}}$  and at a uniform density  $\rho=0.17 \text{ fm}^{-3}$  (see Fig. 11). As in the previous calculation, the initial source is assumed to consist of 24 nucleons. The surface area of the source at the interface with the target spectator region

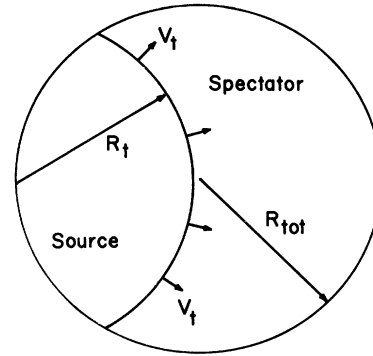


FIG. 11. In the alternate description of the expansion the source expands into the spectator matter with a constant expansion velocity of  $v_t$ .

is assumed to be shadowed; the rest of the source is assumed to emit freely, and possible anisotropies in the emission distribution which may be introduced by shadowing are not considered.

In this expansion description, the shadowing factor  $f$  and the accretion rate  $(dA_s/dt)_a$  are given by

$$f = \left( 3 - \frac{R_t}{R_{\text{tot}}} \right)^{-1} \quad (\text{A13})$$

and

$$\left( \frac{dA_s}{dt} \right)_a = \frac{3R_t^2 v_t}{2r_0^3} \left( 1 - \frac{R_t}{2R_{\text{tot}}} \right). \quad (\text{A14})$$

Energy spectra for carbon fragments at  $\theta_{\text{lab}}=30^\circ$  and  $90^\circ$  corresponding to expansion velocities  $v_t=0.07c$  and  $0.2c$  are shown in Fig. 12. (The Fermi velocity is about  $0.3c$ .) For comparison, the spectrum resulting from the assumption of a constant accretion rate of 2 nucleons/(fm/c) is

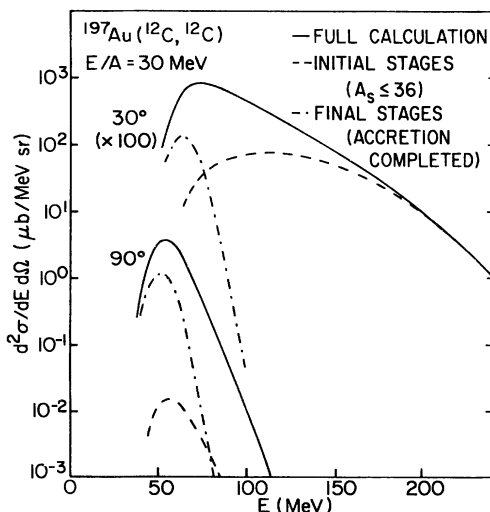


FIG. 10. Decomposition of the final energy spectra for  $^{12}\text{C}$  fragments emitted in  $^{12}\text{C}$  induced reactions on  $^{197}\text{Au}$  at  $E/A = 30 \text{ MeV}$ . The dashed line corresponds to emission from the early stages of the reaction when  $A_s < 36$ . The dashed-dotted line corresponds to emission from the fully equilibrated final stages of the reaction. The solid line corresponds to the complete calculation.

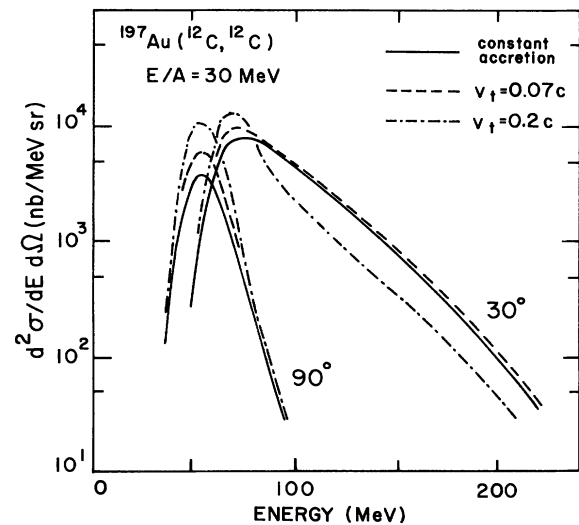


FIG. 12. Calculations of  $^{12}\text{C}$  emission at  $30^\circ$  and  $90^\circ$  from a region growing at a constant rate of 2.0 nucleons per fm/c (solid curves) and with velocities of expansion,  $v_t$ , of  $0.07c$  (dashed curves) and  $0.2c$  (dashed-dotted curves). The normalizations used in the curves are 350, 460, and 460 mb, respectively.

drawn as the solid line. The calculation with  $v_t = 0.07c$  is most similar to the calculation with constant accretion rate and in fact provides an equivalently good description of the data. One might expect to obtain similar agreement with calculations which incorporate alternative geometrical descriptions of the expansion. In general, increasing the expansion rate should increase the relative importance of emission from the equilibrated compound nucleus. This sensitivity may eventually provide valuable information concerning the rate at which the composite system comes to thermal equilibrium.

#### APPENDIX B: BREAKUP OF THE SPECTATOR RESIDUES

The final momentum  $\vec{p}_L$  of the observed fragment in the laboratory frame is calculated as the sum of the following four contributions:

(a) In the rest frame of the spectator matter the prefragments have an isotropic momentum distribution  $F(\vec{p}_F) \sim \exp(-p_F^2/2\Delta_F)$ , which is assumed to be due to the Fermi motion of the target nucleons. If a fragment is broken off suddenly from a target, then the width of its momentum distribution is given by<sup>35</sup>

$$\Delta_F = \frac{k_F^2}{5} \frac{A_T - A_F}{A_T - 1} A_F. \quad (\text{B1})$$

Here,  $k_F$  denotes the Fermi momentum and  $A_T$  and  $A_F$  represent the nucleon numbers of target and fragment, respectively.

(b) Following earlier results<sup>24</sup> we assume that, on the average, each fragment has absorbed one nucleon emitted

from the decaying hot spot. This gives the second contribution to the total fragment momentum. The distribution  $F_2(\vec{p}_N)$  of the nucleon momenta is taken to be a Maxwellian distribution characterized by a temperature  $T$  and an average momentum  $\langle \vec{p}_N \rangle$  in the beam direction.

(c) The fragments are accelerated by the Coulomb field of the spectator matter. In the rest frame of the spectator matter, the final fragment energy is given by

$$E_{\text{final}} = V_C + (\vec{p}_F + \vec{p}_N)^2 / (2M), \quad (\text{B2})$$

where  $V_C$  refers to the Coulomb barrier and  $M$  is the mass of the fragment. Since the fragments are assumed to originate from different locations in the spectator matter having different effective Coulomb barriers, there will be a corresponding distribution  $g(V_C)$  of the Coulomb barriers given by

$$g(V_C) = \frac{V_C^{1/2}}{(V_{C,\text{max}})^{3/2}} \theta(V_{C,\text{max}} - V_C). \quad (\text{B3})$$

$V_{C,\text{max}}$  is the Coulomb barrier for a fragment emitted from the surface of the target nucleus. Further details may be found in Ref. 24.

(d) An additional momentum  $\vec{p}_{\text{c.m.}} = M\vec{v}_{\text{c.m.}}$  is supplied by the transformation from the rest frame of the spectator matter to the laboratory. The velocity  $\vec{v}_{\text{c.m.}}$  of the spectator matter is determined by the momentum transfer to the spectator matter during the formation of the hot spot due to the action of nuclear viscosity.<sup>24</sup>

Assuming that these momentum vectors are uncorrelated, the double differential cross section in the laboratory system is given by

$$\begin{aligned} \frac{d\sigma}{E_{\text{lab}} d\Omega_L dZ} &= C_0(Z_f) \int g(V_C) \delta(\vec{p}_s - \vec{p}_N - \vec{p}_F) F_1(p_F) F_2(p_N) M p_L y d^3 p_N d^3 p_F dV_C \\ &= C_0(Z_f) \int \frac{(ab)^{3/2}}{\pi^3} g(V_C) e^{-a\langle \vec{p}_N \rangle - bp_s^2 - (a+b)p_N^2 + 2p_N(\langle b\vec{p}_s + a\langle \vec{p}_N \rangle) \cos x} 2\pi y M p_N^2 p_L dp_N d\cos x dV_C, \quad (\text{B4}) \end{aligned}$$

where

$$a = \frac{1}{2} m_{\text{nucleon}} T, \quad (\text{B5})$$

$$b = \frac{1}{2} \Delta_F. \quad (\text{B6})$$

$C(Z_f)$  is a normalization constant,  $T$  is the temperature of the hot spot, and  $p_s$ , the fragment momentum at the surface of the spectator matter in the rest frame of the spectator matter, is given by

$$\begin{aligned} \vec{p}_s &= [1 - 2MV_C / (\vec{p}_L - \vec{p}_{\text{c.m.}})^2]^{1/2} (\vec{p}_L - \vec{p}_{\text{c.m.}}) \\ &= y (\vec{p}_L - \vec{p}_{\text{c.m.}}). \quad (\text{B7}) \end{aligned}$$

The momentum vectors, however, are not completely uncorrelated. In fact, the small size of the hot spot results in a correlation between the momentum of the absorbed hot spot nucleon and the final momentum of the fragment as shown in Fig. 13. One can incorporate this correlation by replacing  $d\cos x$  in Eq. (B4) by  $f(\cos x) d\cos x$ , where

$f(\cos x)$  describes the correlation. We obtain  $f(\cos x)$  by making the following approximations:

(1) The fragments are assumed to come from the surface region of the spectator matter. Hence,  $|\vec{l}| \approx |\vec{R}|$ .

(2)  $\vec{p}_s$  is taken to be parallel to  $\vec{R}$  corresponding to the most probable escape trajectory.

(3) We neglect the finite size of the hot spot. Rather we assume that all hot spot nucleons originate from the center of the hot spot. Then we can replace  $f(\cos x)$  by  $|a\delta(\cos x - \cos \bar{x})|$  ( $a$  is a constant), where

$$\bar{x} = \arcsin \left[ \frac{\tilde{p}_{\parallel}}{p_H} \sin \gamma \right] - \gamma / 2$$

and

$$\tilde{p}_{\parallel} = a \langle p_N \rangle.$$

Equation (B4) contains five parameters [ $\langle \vec{p}_N \rangle$ ,  $T$ ,  $\vec{p}_{\text{c.m.}}$ ,  $C(Z_f)$ , and  $V_{C,\text{max}}$ ] which have been determined by fit-

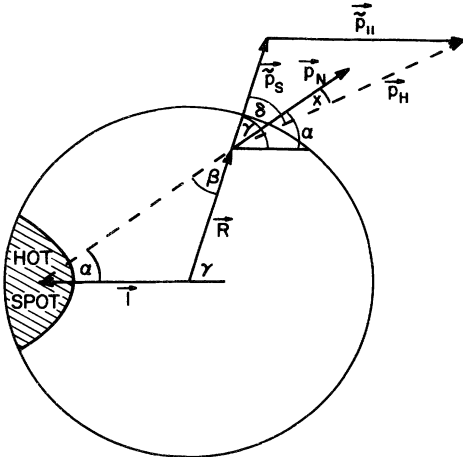


FIG. 13. Geometrical assumptions used for evaluating the interaction of participant nucleons with the spectator matter. The incoming projectile interacts violently with some target nucleons to form a hot spot of very limited spatial extent. This hot spot decays primarily by emitting nucleons which traverse the cold target matter for small impact parameters and destabilize the target which leads to the formation of fragments. The momentum in the rest frame of the spectator matter of a fragment located at  $R$  is given by  $\vec{p}_s = \vec{p}_N + \vec{p}_F$ , where  $\vec{p}_N$  is the momentum of the hot spot nucleon which is absorbed by fragment and  $\vec{p}_F$  is the random momentum due to Fermi motion. As discussed in the text, this geometry leads to a constraint upon the angle  $\alpha$  between  $\vec{p}_N$  and  $\vec{p}_H = \vec{p}_s + \vec{p}_{||}$  (note the following:  $\vec{p}_{||} = a\vec{p}_{||}$ ;  $\vec{p}_s = b\vec{p}_s$ ;  $a$  and  $b$  are discussed in the text).

ting the experimental data. The parameters  $\langle \vec{p}_N \rangle$ ,  $T$ , and  $p_{c.m.}/M$  are assumed to be the same for all fragments and were determined by fitting the energy spectrum for  $Z_f=8$ .  $V_{C,max}$ , the maximal Coulomb barrier of the fragment, is related to a distance  $R_{max}$  between the centers of the target and the outgoing fragment by  $R_{max} = \epsilon(R_{target} - R_{fragment})$ . For emission from the surface of a spherical spectator region,  $\epsilon=1$ , whereas  $\epsilon > 1$  is expected for deformed fragments. The energy spectra from high energy nucleus-nucleus reactions are consistent with an  $\epsilon$  of 1.18.<sup>24</sup> We adopt this value of  $\epsilon$  in our calculation.  $C_0(Z_f)$  is then a normalization constant which is separately determined for each fragment by fitting the spectra with  $C_0(Z_f)$  as a free parameter and using the values for  $T$ ,  $\langle \vec{p}_N \rangle$ , and  $\vec{p}_{c.m.}$  which had been determined from a fit of the spectrum for  $Z_f=8$ .

In high energy reactions the dependence of the elemental cross sections upon  $Z_f$  have been described in a model in which conservation of charge is imposed upon the principle of minimum information. For details, we refer to Ref. 23. In this model, the elemental cross section assumes the form

$$\sigma(Z_f) = \sigma_0 \frac{1}{\exp(1.28Z/\sqrt{Z_0}) - 1}, \quad (B8)$$

where  $Z_0$  is the total charge of the system after the emission of the preequilibrium light particles. When Eq. (B8) is applied to the present data, the elemental cross sections  $\sigma(Z_f)$  are well described by  $Z_0=20$ , which is considerably smaller than the total charge of the target spectator.

\*On leave from University of Heidelberg, Heidelberg, Federal Republic of Germany.

<sup>1</sup>A. M. Poskanzer, G. W. Butler, and E. K. Hyde, Phys. Rev. C 3, 882 (1971).

<sup>2</sup>G. D. Westfall, R. G. Sextro, A. M. Poskanzer, A. M. Zebelman, G. W. Butler, and E. K. Hyde, Phys. Rev. C 17, 1368 (1978).

<sup>3</sup>B. D. Wilkins, S. B. Kaufman, E. P. Steinberg, J. A. Urbon, and D. J. Henderson, Phys. Rev. Lett. 43, 1080 (1979).

<sup>4</sup>J. A. Gaidos, L. J. Gutay, A. S. Hirsch, R. Mitchell, T. V. Ragland, R. P. Scharenberg, F. Turkot, R. B. Willmann, and C. L. Wilson, Phys. Rev. Lett. 42, 82 (1979).

<sup>5</sup>R. E. L. Green and R. G. Korteling, Phys. Rev. C 22, 1594 (1980).

<sup>6</sup>J. E. Finn, S. Agarwal, A. Bujak, J. Chuang, L. J. Gutay, A. S. Hirsch, R. W. Minich, N. T. Porile, R. P. Scharenberg, B. C. Stringfellow, and F. Turkot, Phys. Rev. Lett. 49, 1321 (1982).

<sup>7</sup>R. W. Minich, S. Agarwal, A. Bujak, J. Chuang, J. E. Finn, L. J. Gutay, A. S. Hirsch, N. T. Porile, R. P. Scharenberg, B. C. Stringfellow, and F. Turkot, Phys. Lett. 118B, 458 (1982).

<sup>8</sup>K. A. Frankel and J. D. Stevenson, Phys. Rev. C 23, 1511 (1981).

<sup>9</sup>U. Lynen, H. Ho, W. Kühn, D. Pelte, U. Winkler, W. F. J. Müller, Y.-T. Chu, P. Doll, A. Gobbi, K. Hildenbrand, A. Olmi, H. Sann, H. Stelzer, R. Bock, H. Lohner, R. Glasow, and R. Santo, Nucl. Phys. A387, 129c (1982).

<sup>10</sup>H. H. Gutbrod, A. I. Warwick, and H. Wieman, Nucl. Phys.

A387, 177c (1982).

<sup>11</sup>A. I. Warwick, A. Baden, H. H. Gutbrod, M. R. Maier, J. Péter, H. G. Ritter, H. Stelzer, H. H. Wieman, F. Weik, M. Freedman, D. J. Henderson, S. B. Kaufman, E. P. Steinberg, and B. D. Wilkins, Phys. Rev. Lett. 48, 1719 (1982).

<sup>12</sup>A. I. Warwick, H. H. Wieman, H. H. Gutbrod, M. R. Maier, J. Péter, H. G. Ritter, H. Stelzer, F. Weik, M. Freedman, D. J. Henderson, S. B. Kaufman, E. P. Steinberg, and B. D. Wilkins, Phys. Rev. C 27, 1083 (1983).

<sup>13</sup>B. V. Jacak, G. D. Westfall, C. K. Gelbke, L. H. Harwood, W. G. Lynch, D. K. Scott, H. Stocker, M. B. Tsang, and T. J. M. Symons, Phys. Rev. Lett. 51, 1846 (1983).

<sup>14</sup>C. B. Chitwood, D. J. Fields, C. K. Gelbke, W. G. Lynch, A. D. Panagiotou, M. B. Tsang, H. Utsunomiya, and W. A. Friedman, Phys. Lett. 131B, 289 (1983).

<sup>15</sup>S. Bohrmann, J. Hüfner, and M. C. Nemes, Phys. Lett. 120B, 59 (1983).

<sup>16</sup>J. Hüfner and H. M. Sommermann, Phys. Rev. C 27, 2090 (1983).

<sup>17</sup>W. A. Friedman and W. G. Lynch, Phys. Rev. C 28, 950 (1983).

<sup>18</sup>D. H. E. Gross, L. Satpathy, Meng Ta-chung, and M. Satpathy, Z. Phys. A 309, 41 (1982).

<sup>19</sup>J. Randrup and S. E. Koonin, Nucl. Phys. A356, 223 (1981).

<sup>20</sup>G. Fai and J. Randrup, Nucl. Phys. A381, 557 (1982).

<sup>21</sup>J. P. Bondorf, Nucl. Phys. A387, 25c (1982).

<sup>22</sup>D. Boal, Phys. Rev. C 28, 2568 (1983).

- <sup>23</sup>J. Aichelin and J. Hüfner, *Phys. Lett.* **136B**, 15 (1984).
- <sup>24</sup>J. Aichelin, J. Hüfner, and R. Ibarra, *Phys. Rev. C* **30**, 107 (1984).
- <sup>25</sup>J. Barrette, P. Braun-Munzinger, and C. K. Gelbke, *Nucl. Instrum. Methods* **126**, 181 (1975).
- <sup>26</sup>U. Littmark and J. F. Ziegler, *Handbook of Range Distributions for Energetic Ions in All Elements* (Pergamon, New York, 1980).
- <sup>27</sup>A. L. Goodman, J. I. Kapusta, and A. Z. Mekjian, Lawrence Berkeley Laboratory Report LBL-16471.
- <sup>28</sup>T. C. Awes, G. Poggi, C. K. Gelbke, B. B. Back, B. G. Glagola, H. Breuer, and V. E. Viola, Jr., *Phys. Rev. C* **24**, 89 (1981).
- <sup>29</sup>T. C. Awes, G. Poggi, S. Saini, C. K. Gelbke, R. Legrain, and G. D. Westfall, *Phys. Lett.* **103B**, 417 (1981).
- <sup>30</sup>T. C. Awes, S. Saini, G. Poggi, C. K. Gelbke, D. Cha, R. Legrain, and G. D. Westfall, *Phys. Rev. C* **25**, 2361 (1982).
- <sup>31</sup>G. D. Westfall, B. V. Jacak, N. Anantaraman, M. W. Curtin, G. M. Crawley, C. K. Gelbke, B. Hasselquist, W. G. Lynch, D. K. Scott, M. B. Tsang, M. J. Murphy, T. J. M. Symons, R. Legrain, and T. J. Majors, *Phys. Lett.* **116B**, 118 (1982).
- <sup>32</sup>A. S. Goldhaber, *Phys. Rev. C* **17**, 2243 (1978).
- <sup>33</sup>W. G. Lynch, C. B. Chitwood, M. B. Tsang, D. J. Fields, D. R. Klesch, C. K. Gelbke, G. R. Young, T. C. Awes, R. L. Ferguson, F. E. Obenshain, F. Plasil, R. L. Robinson, and A. D. Panagiotou, *Phys. Rev. Lett.* **51**, 1850 (1983).
- <sup>34</sup>W. A. Friedman and W. G. Lynch, *Phys. Rev. C* **28**, 16 (1983).
- <sup>35</sup>A. S. Goldhaber, *Phys. Lett.* **53B**, 306 (1974).